Second-order optical effects in organometallic nanocomposites induced by an acoustic field

A. Migalska-Zalas and B. Sahraoui

Laboratoire POMA UMR CNRS 6136, Université d'Angers, 2. Boulevard Lavoisier 49045 Angers, France

I. V. Kityk and S. Tkaczyk

Institute of Physics, J. Dlugosz Academy of Częstochowa, PL-42217, Aleja Armii Krajowej 13/15, Częstochowa, Poland

V. Yuvshenko

The Scientific Research Corporation ALCOR, pr. Nauki 25, Kyiv, Ukraine

J.-L. Fillaut and J. Perruchon

Institut de chimie de Rennes, Université Rennes I and UMR CNRS 6509 Laboratoire Organométalliques et Catalyse, 35042 Rennes Cedex, France

T. J. J. Muller

Organisch-Chemisches Institut, Universität Heidelberg, 69120 Heidelberg, Germany

Acoustically stimulated second-order optical effects in Ru-derivative nanocomposites were discovered. The alkynyl ruthenium derivatives were embedded in a polymethyl methacrylate (PMMA) polymer matrix. As second-order optical effects we studied second-harmonic generation (SHG) and linear electro-optics (LEO) phenomena. The physical insight of the effect observed consists in a coexistence of nanocofined chromophore levels and localized d states of ruthenium. A transverse acoustic field favors the occurrence of charge density noncentrosymmetry required for observation of the second-order optical effects, particularly SHG. We have found that acoustically induced SHG and LEO for fundamental YAB-Gd^{3+} laser light ($\lambda = 1.76$ μm) increases and achieves a maximum value at acoustic power density of about 1.45 W/cm^2. The values of the SHG for several Ru chromophores were higher than those for well-known inorganic crystals. With decreasing temperature, the SHG signal strongly increases below 55 K and correlates well with occurrence of "softlike" low-frequency anharmonic quasiphonon modes responsible for the phase transitions. The SHG maxima were observed at acoustic frequencies of about 13 kHz. Increasing of acoustical frequencies up to the megahertz range suppresses the observed phenomena. Comparing the obtained results with the acoustically induced Raman spectra at different temperatures one can conclude that the observed effects are due to acoustically induced electron-vibration anharmonicity, and are observed at temperatures below 55 K. Varying the chromophore content within the embedded matrices we were able to use effective nanoparticle sizes within the range 5–60 nm. It is clearly shown that the enhancement of the effective nanosize effectively suppresses the observed second-order optical effects.

PACS number(s): 42.70.Mp

I. INTRODUCTION

Optical second-harmonic generation (SHG) induced by an acoustical field was first observed in Ref. 1. Similar phenomena were also observed in several composites, both in bulk as well as in large-sized nanocrystallite samples.[2,3] The effect is generally explained by a noncentrosymmetric spatial charge density distribution of photocarrier excitation under an external acoustical field[4] due to electrostriction (photoacoustical) effects. Existence of charge density noncentrosymmetry is a necessary condition for observation of second-order optical effects described by third-rank polar tensors. This effect can be explained within a framework of interaction of electron-hole and electron-phonon subsystems resulting in acentric output of the charge density distribution. One can guess that incorporated organometallic chromophores in an optically transparent and electrically neutral matrix like polymethyl methacrylate (PMMA) polymers may be considered a promising way to obtain second-order optical effects induced by

an external acoustic field. We have chosen ruthenium alkynyl derivatives, which are currently the subject of increasing attention due to the large nonlinear optical (NLO) response which they can possess due to d-π charge transfer.[5] Analogously to ferrocene, the metal acts as the donor group. Moreover, the presence of the Ru atoms could give enhancement in low-frequency quasiphonon (vibration) modes ("soft" modes), which determine anharmonic electron-phonon interactions.[6–8]

In this experiment we have investigated the SHG and linear electro-optics (LEO) in a series of ruthenium alkynyl systems, particularly versus acoustic power, frequency, and temperature. Guest-host chromophores are being widely investigated and the observed SHG could be an additional motivation for their detailed study, particularly concerning the electron-phonon anharmonic interactions. Comparison with several other photorefractive ferroelectric crystals will be discussed.
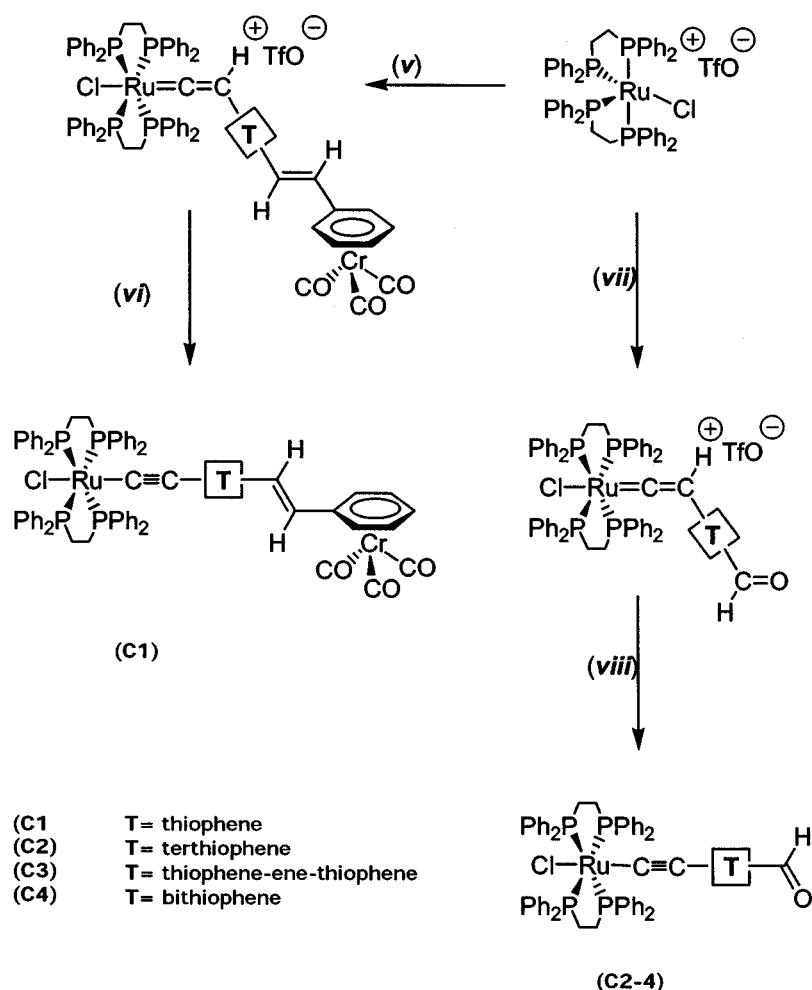
FIG. 1. Synthetic procedures to obtain the alkynyl derivatives (v) [RuCl(dppe)$_2$][TfO] 0.25 mmol, A1 0.30 mmol, CH$_2$Cl$_2$ 40 mL, room temperature (RT) 20 h; (vi) 1,8-diazabicyclo[5.4.0]undec-7-ene (DBU) 0.50 mmol, CH$_2$Cl$_2$ 40 mL, RT, 1 h; (vii) [RuCl(dppe)$_2$][TfO] 0.50 mmol, A2–4 0.60 mmol, CH$_2$Cl$_2$ 50 mL, RT, 20 h; (vii) Et$_3$N 1 mmol, CH$_2$Cl$_2$ 20 mL, RT, 1 h.

(C1)	T= thiophene
(C2)	T= terthiophene
(C3)	T= thiophene-ene-thiophene
(C4)	T= bithiophene

II. EXPERIMENTAL DETAILS

A. Sample preparation

The synthesis of alkynyl complexes C1 and C2–4 (Fig. 1) was performed by the method described in Ref. 9. The synthesis of the new alkynes (A1 and A2–4) follows the procedure outlined in Fig. 2. Sonogashira coupling,[10] which was used to prepare the trimethylsilyl-protected alkynes Si1–4 in good yields which were then reacted in the standard manner to give the teminal alkynes A1–4. Isolation of the trimethylsilyl-protected alkyne intermediates Si2–4 offered no advantage in terms of yield and purity. An advantage in purity and yield of the final product A1 was achieved by isolating the trimethylsilyl-protected alkyne Si1 and reacting it with the arene chrome tricarbonyle phosphonate anion (Horner-Emmons-Wadsworth coupling[11]) prior to the deprotection step. Reaction of this anion with the terminal alkynes 1 afforded a lower yield of 3, along with several unidentified by-products. These new alkynes were fully characterized by NMR methods.

The obtained chromophore molecules were incorporated into the PMMA matrix. The investigated samples were prepared as a mixture of 4 g of PMMA and 0.035 g of chromophore and dissolved in 30 mL of chloroform in an argon atmosphere. This mixture was prepared using a magnetic stirrer and they were put in an alumina crucible after that.

One of the complications of the complexes investigated is their partial photodestruction under influence of laser light. Specially performed NMR and ir investigations have shown that under the influence of laser light, particularly of power density higher than 450 MW/cm^2 a little destruction of the chromophore has occurred; however, in the PMMA matrix this degradation does not exceed 7.2%, and the major part of the molecule participated in the desired processes. Varying the concentration of the dopants within 3.5–7 % we were able to use effective sizes of the nanoparticles within the range 5–60 nm. The investigated composite samples had the form of parallelepipeds with dimensions of about $3 \times 3 \times 0.7$ mm.^{3}

The chemical structure of the studied compounds and their uv spectra are presented in Table I.

B. Measurement setup

The principal setup for the SHG and LEO measurements is shown in Fig. 3. A pulsed mode-locked Dy^{3+}:YAB laser ($\lambda = 1.76$ μm) was used to avoid a possible spectral overlap with luminescence of the chromophore. The gadollimium-doped yttrium aluminum garnet (Gd:YAG) laser had the following parameters: pulse power density 2.5 MW; pulse time duration 15 ps; frequency repetition 15 Hz; beam spot diameter 1.8 mm. The samples had refractive indices 1.51 and
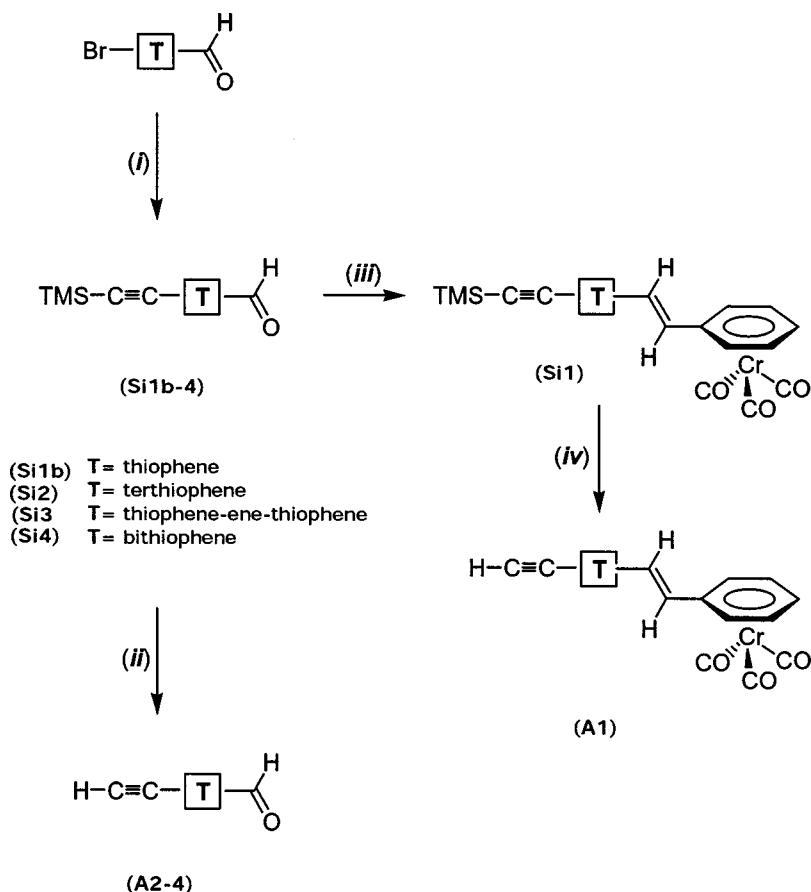
FIG. 2. General access to the terminal alkynes A1–4 (i) PdCl$_2$(PPh$_3$)$_2$, CuI, trimethylsilylacetylene, THF, Et$_3$N, 50 °C, 24 h; (ii) Bu$_4$NF (solution 1M in THF), 1 eq. THF, RT, 1 h; (iii) [Cr(CO)$_3$(η^6-C$_6$H$_5$)CH$_2$P(O) $\times$(OCH$_3$)$_2$], 1.1 eq. NaH, THF, 12 h, 65 °C, (iv) Bu$_4$NF (solution 1M in THF), 2 eq. THF, RT, 1 h.

1.62 for the fundamental and doubled laser beam frequency, respectively. These parameters were controlled by the Obreimov method. The induced birefringence was measured by the traditional Senarmont method and was less than 10^{-3}.

The acoustic power was applied to investigate composites using a LiNbO$_3$ piezoelectric acoustic transducer (AT), allowing varying the frequencies within the spectral range 1 Hz–1.1 MHz. The acoustical transducer was glued to the surface of the sample. The setup allowed the transfer of up to 46% of the acoustic power to the composite. The angle between the composite surface and incident beam direction Φ was changed to obtain the angle dependencies of the SHG within the Maker fringe scheme.

Using an attenuator A (see Fig. 3) we were able to vary the power density within the range 0.1–2.5 MW per pulse. It was particularly important during measurements of the LEO. In this case we have used the traditional Senarmont scheme for measurement of the Pockels effect. Applying an electric field E with frequency up to hundreds of kilohertz and amplitudes about 2 kV we have determined LEO effects within a Senarmont scheme using the polarizer P1, and analyzer P2 together with a $\lambda/4$ plate supplied to monitor the angle necessary for compensation of the transparent light passing through the system of the crossed polarizers. The birefringence was determined from the equation

$$\Delta n_\theta = \frac{\lambda \varphi}{d_\theta}, \qquad (1)$$

where φ is the measured angle for the given wavelength λ and the effective sample thickness is d_θ.

The incident laser beam was polarized using polarizer P1 (with degree of polarization of about 99.997%) and the output doubled-frequency SHG light intensities were detected using photomultiplier PM1 connected with a 690 ps gate electronic boxcar. The short-time pulse duration allowed avoiding an increase of local temperature. The laser beam was spatially filtered in order to obtain a homogeneous light profile (usually a Gaussian-like shape profile sequence) possessing per-pulse-energy power densities varying within the 0.6–1.2 GW/cm^2 range. A grating spectrophotometer SP separated the fundamental beam of the Gd^{3+}:YAB laser (λ =1.76 μm) from the SHG (λ=0.88 μm) as well as from the scattered background. For incident and output beam energies, monitoring photomultipliers PM1 and PM2 connected to the computer PG were used.
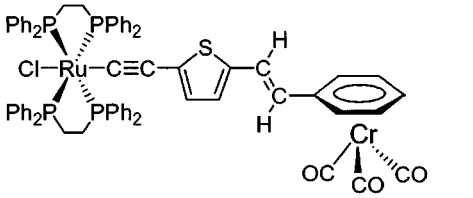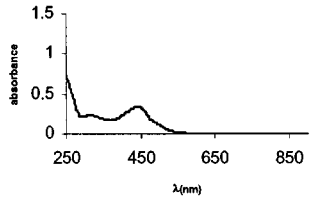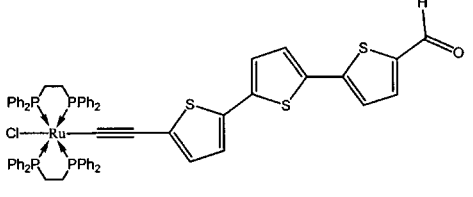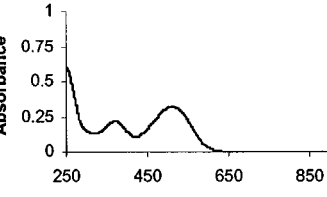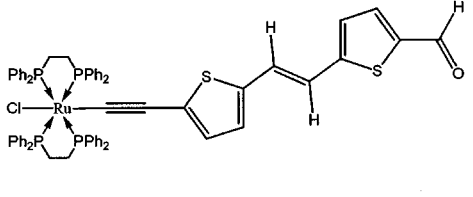
During evaluation of the second-order nonlinear optical response χ_{ijk} we measured light intensities I for the ω and 2ω laser frequencies. The evaluation of the nonlinear optical susceptibility χ_{ijk} was performed using a method described in Refs. 3 and 12.

We have performed evaluations by taking into account the angle-dependent birefringence Δn_θ and changes of thickness d_θ by applying the following expression:

$$I = I_0 \sin^2(\pi \Delta n_\theta d_\theta / \lambda) \qquad (2)$$

where I and I_0 are the output and incident light intensities, respectively. The polarization of the optical beam was parallel to the polarization of the acoustic wave polarization for

TABLE I. Chemical structure of the studied compounds and their uv spectra.

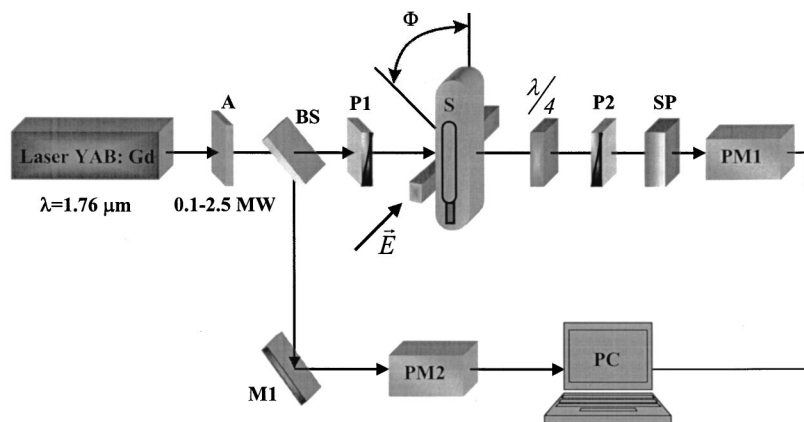| *Studied compounds*	*Spectra*
C1	
C2	
C3	
C4	
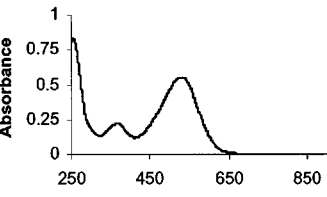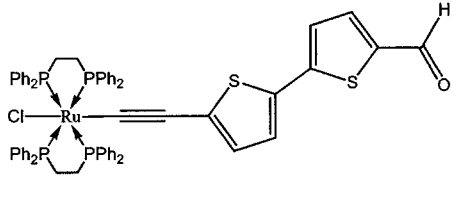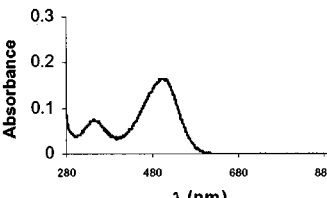
FIG. 3. Principal schema of the acoustically stimulated SHG experiment, BS, beam splitter; M1, M2, mirrors; P1, P2, polarizers; A, attenuator; S, specimens kept in liquid helium cryostat; SP, spectrograph; PM1, PM2, photomultipliers; PC, personnal computer; DL, delaying line; Φ, complement of the angle of incidence onto the sample; E, applied electric field.
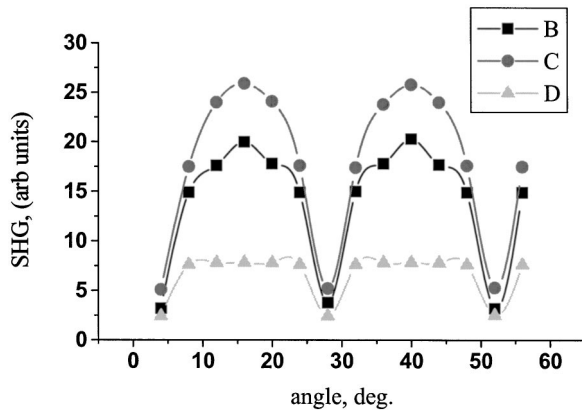
FIG. 4. Typical dependences of the acoustically induced optical SHG versus the effective specimen thickness at acoustical frequency 13 kHz and different acoustical powers: curve B, 0.79 W/cm^2; curve C, 1.75 W/cm^2 for the C4 sample for averaged nanoparticle size about 5 nm. The curve D shows the same at acoustical power about 1.75 W/cm^2 and averaged nanoparticle size about 50 nm. All the measurements are done at $T=4.2$ K.

every angle θ between the laser beam propagation and composite's surface.

To monitor the possible phase transitions we applied the differential scanning calorimetric (DSC) method, which is sensitive to structural transitions or chemical transformations. Our equipment consisted of a Netzsch STA 406C DSC instrument with low-temperature controller TASC 414/3 (Netzsch), stabilizing the cooling rate process. The powder-like sample was put in an Al$_2$O$_3$ crucible. The sample was cooled from ambient temperature to 4.2 K in an argon atmosphere with a rate of 0.18 K per min and thermostabilization of up to 0.1 K. We performed measurements during both cooling and heating regimes to achieve additional control of possible ferroelectric spontaneous polarization P_s occurrence. The traditional Tower-Sower method gave the possibility to evaluate P_s with precision up to 0.5 μC/cm^2. Additionally we have measured Raman scattering spectra using a Kr laser ($\lambda=745$ nm) as a light source. We have indicated the chromophores by special letters for our convenience (see Table I).

III. RESULTS AND DISCUSSION

All the observed SHG dependences have shown similar behavior versus the angle between the beam propagation and the normal to the sample surface. Typical Maker fringence angle dependencies of the SHG at different acoustical power densities versus effective thickness for compound C4 are shown in Fig. 4. The Maker fringe oscillations (see Fig. 4) are enhanced by intensities with increasing acoustical power. At the same time for the enhancement of averaged nanoparticle sizes up to about 50 nm the effect drastically decreases due to chromophore particle agglomeration.

Maximal output SHG intensities were achieved for parallel directions of the transverse acoustical wave displacement and polarization of the incident laser beam.
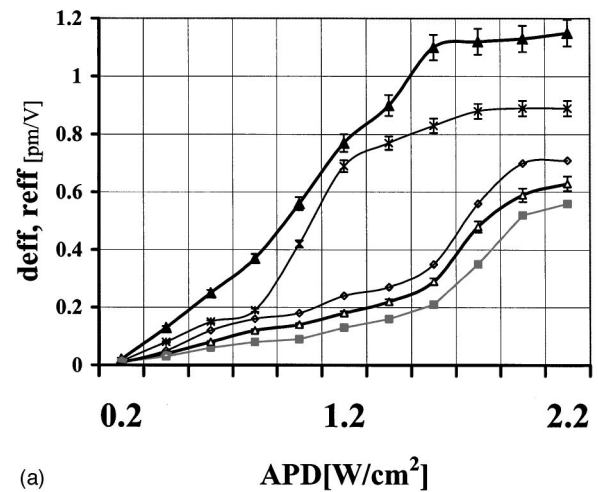
(a)
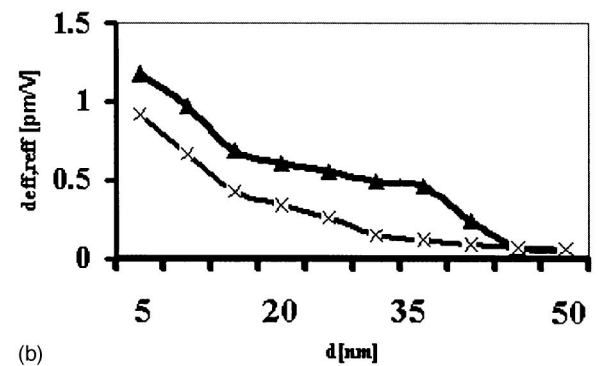
(b)

FIG. 5. (a) Dependence of the SHG and LEO on the acoustical power for different samples: SHG, C1 ($\triangle$), C2 ($\blacksquare$), C3 ($\diamond$), C4 ($\times$); LEO, ($\blacktriangle$) for C4. (b) Dependences of the effective second-order optical susceptibility defined from the SHG ($\times$) and LEO ($\blacktriangle$) versus averaged nanoparticle sizes for the C4 samples at 13 kHz and temperature about 5 K.

We varied effective thickness of the sample by rotating it with respect to the light beam propagation. For each angle, the appropriate light power components were evaluated, taking into account Fresnel losses and the projection of the effective optical path as well as birefringence. To simplify the evaluation, final measurements were done for parallel directions of the acoustic wave polarization (acoustic field displacement) and probing light polarization beams. The accuracy of determination of nonlinear optical susceptibility after such procedure was equal to about 0.1 pm/V. As a SHG reference sample we have used a single crystal of potassium dihydrogen phosphate (KDP).

Dependences of the SHG on the acoustic power density are generally nonlinear [see Fig. 5(a)]. One can clearly see that maximum increase of the SHG is observed at acoustic power densities of 1–1.7 W/cm^2. Increasing differences for C4 compared C3, C2, and C1 exist. We present the SHG behavior corresponding to the maximum SHG output which was achieved at temperature about 4.2 K and acoustic frequency about 13 kHz. It is necessary to emphasize that at megahertz frequencies the effect disappears. The value of the effective LEO coefficient demonstrates almost a similar dependence versus acoustical field as the SHG.
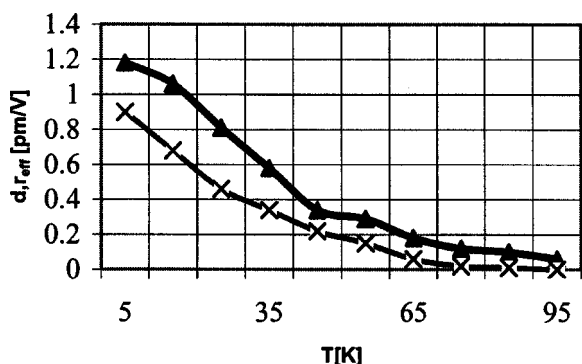
FIG. 6. Typical dependences of the SHG ($\times$) and LEO ($\blacktriangle$) versus the temperature at optimal conditions.

From Fig. 5(a), one can see also several slight kinks in the corresponding acoustic power dependences. These kinks may indicate the contribution of anharmonic electron-phonon interactions, similarly as in Refs. 2 and 3. Following the general theory of anharmonic electron-phonon interactions one can expect that these effects may be enhanced during different kinds of phase transformations.[6] It is crucial that in the case of acoustic excitation we deal with changes of macrosymmetry due to occurrence of an interaction between the acoustic wave branches and the lowest quasiphonon modes. Due to the transverse symmetry of acoustic waves there occurs the possibility of creating a charge density noncentrosymmetry.

In Fig. 5(b) there are presented additionally the dependences of d_{eff} and r_{eff} versus averaged nanoparticle sizes. Below 45 nm the effect almost disappears.

The performed temperature measurements of the SHG have demonstrated that a large increase of the SHG is observed below 55 K [see Fig. 6(a)]. To study the origin of the observed SHG and LEO enhancement we have done additional measurements using the DSC method. Comparing the temperature dependences of the SHG, LEO, and DSC (see Figs. 6 and 7) one can see a sufficiently good correlation of the particular extrema of the DSC and the bending in the SHG dependences. It means that the observed increase of the SHG at temperatures below 55 K is caused by a phase transformation that, in this case, does not possess temperature hysteresis.

Phase transitions were also studied by Raman spectroscopy (see Fig. 8) at different applied acoustical powers for additional clarification of the electron-phonon anharmonic contributions. With increasing acoustical power the intensi-
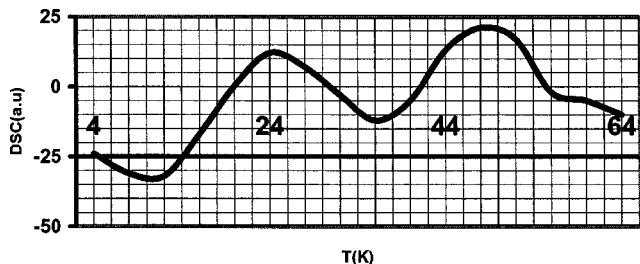
FIG. 7. Temperature-dependent DSC signal $\times 10^3$ for the sample C4 achieved at the optimal conditions.
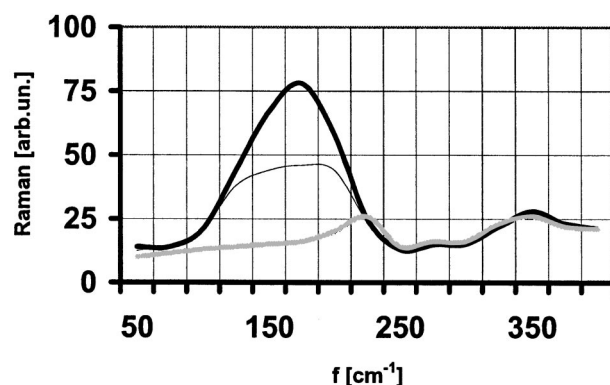
FIG. 8. Behavior of the acoustically induced Raman modes at $T=5$ K at different acoustical powers for C4: thin black line, 0.65 W/cm^2; thick black line, 1.75 W/cm^2 at 13 kHz acoustical frequencies. The gray line corresponds to the frequencies of the acoustical field about 1 MHz. All the measurements are done at the optimal conditions for the second-order optical susceptibilities.

ties of the Raman modes around 170 cm^{-1} also increase. The analysis of the origin of the vibration modes was done using the semiempirical AM1 method within the quantum chemical package HYPERCHEM 7.0. We have established that the anharmonic modes originate from simple superposition of Ru-O and Cr-O in the case of its presence, from the performed evaluations. The noncentrosymmetric vibration modes with frequencies 310 and 387 cm^{-1} possess relatively strong oscillator strengths. In the vicinity of the phase transitions, the oscillator strengths of the corresponding modes should increase due to increasing electron-phonon anharmonicity. It is necessary to emphasize that outside the phase transition region we do not observe an increase of the corresponding mode intensities. The enhancement of the acoustical power up to 1 MHz leads to suppression of the corresponding anharmonic vibration modes.

Direct measurements of the spontaneous polarization P_s near the critical temperature points did not indicate the occurrence of spontaneous polarization P_s with decreasing temperature. So the phase transition mentioned has a nonferroelectric origin.

The degree of the noncentrosymmetry is proportional to the third-order nonlinear optical susceptibilities similarly to electric-field-induced optical SHG. Simultaneously during the phase transitions we have displacements of particular ions from their equilibrium positions (particularly due to condensation of the "soft" phonon modes[7]). The latter factor explains additional contribution of the atom-displaced polarizations to the total noncentrosymmetry. Such behavior is similar to the optical SHG temperature dependences during a structural phase transition.

Finally we present (see Fig. 9) the acoustical frequency dependences of the output SHG and LEO for the acoustical power 1.75 W/cm^2. We revealed d_{eff} maxima at frequencies about 13 kHz and above 42 kHz. During the measurements, we simultaneously monitored the efficiency of acoustical interaction with the sample using the echo-pulse method. Without the acoustical field the SHG signal is substantially smaller and its behavior is substantially different.
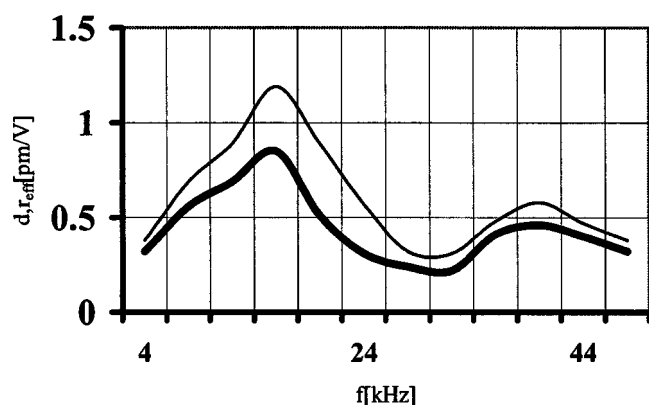
FIG. 9. Dependence of the acoustically induced second-order nonlinear optical susceptibility tensor component d_{yyy} SHG versus the acoustical frequency at acoustical power 1.75 W/cm^2 for the compound C1 at $T = 5$ K.

The clear frequency-dependent behavior together with the above Raman data and the absence of spontaneous polarization unambiguously indicate a domination of acoustically induced electron-phonon interactions in the phenomena observed.

The experimental data presented (see Figs. 4–9), particularly nonlinear dependences versus the acoustical power, as well as the sensitivity to low-temperature phase transformations, indicate that the origin of the observed phenomenon is caused by the acoustically induced quasiphonons, effectively interacting with the electron subsystems. The interaction has an electrostricted nature and favors an acentric charge density distribution similarly to the SHG observed under an influence of the electron beam.[2,3]

The second-order nonlinear optical effects are described by the third-order polar tensors. The latter are especially large in ferroelectrics.[3] In our case this possibility should be excluded. Concerning the contributions due to the electrostriction effect, it should be emphasized that the effect may be observed also in centrosymmetric media due to fourth-rank tensor symmetry.

We also have made similar SHG measurements for several typical ferroelectric and photorefractive crystals. By varying acoustical powers, strengths, and frequencies at different temperatures we have evaluated the corresponding second-order susceptibilities (see Table II).

In Table II maximally achieved values of SHG are presented. They clearly show that the obtained susceptibility values are higher than for typical photorefractive materials. At the moment it is difficult to perform a direct comparison with the structure of the particular organic chromophore due to possible destruction of the molecule within the matrices.

One can see that the Ru derivatives possess the highest acoustically stimulated SHG among the well-known ferroelectric and photorefractive crystals. This might be a consequence of the simultaneous presence of strong electron-

TABLE II. Typical values of the acoustically induced SHG for several ferroelectric and photorefractive crystals.

Type of sample	Maximal AlO SHG value (pm/V) (temperature at which it is achieved)
$Bi_{12}SiO_{20}$ (Ref. 3)	0.06 (96 K)
$Ba_2NaNb_5O_{15}$ (Ref. 3)	0.17 (106 K)
$Bi_4Ge_3O_{12}$ (Ref. 3)	0.36 (153 K)
$LiNbO_3$ (Ref. 3)	0.12 (92 K)
$PbGe_3O_{14}$ (Ref. 3)	0.24 (35 K)
C4	0.80 (4.2 K)
PGB (Ref. 3)	0.61 (4.2 K)

quasiphonon anharmonic interaction typical for the solid-state alloys and the presence of transition metals (Ru or Cr). The latter is caused by low-energy vibration modes stimulated by an external low-frequency transverse acoustic field. The stimulated nanoconfined quasiphonons in molecules of nanosize (up to 3 nm) related to the localized d states of Ru may play here a crucial role. As a confirmation of this fact it should be emphasized that in the case of the agglomeration of the chromophore (increase of effective nanosize) the effect disappeared and replacement of Ru by other metals like Zn drastically reduces the effect.

The present report presents experimental results which require substantial theoretical support. This work is now in progress and will be the subject of a separate work.

IV. CONCLUSIONS

The occurrence of second-order optical susceptibility in Ru-derivative nanocomposites was discovered under the influence of a low-frequency (about 13 kHz) acoustic field. The physical meaning of the effect observed is explained by the coexistence of nanoco-fined chromophore levels and localized d states of ruthenium.

The observed effect was maximal for parallel directions of the acoustic displacement field and fundamental light beam polarization. The significant increase of the SHG below 55 K and its correlation with the DSC data indicates a crucial role of electron-phonon anharmonicity stimulated by an external acoustic field in the observed phenomenon. The investigated Ru possesses higher second-order susceptibilites compared to the known ferroelectric and photorefractive crystals. This might be the consequence of simultaneous presence of strong electron-quasiphonon anharmonic interaction typical for solid-state alloys and the presence of transition metals (Ru or Cr) stimulated by external fields. As a confirmation of this fact it should be emphasized that in the case of the agglomeration of the chromophore the effect disappears and replacement of the Ru by other metals like Zn drastically reduces the effect.

[1] G. D. Boyd, F. R. Nash, and D. F. Nelson, Phys. Rev. Lett. **24**, 1298 (1970); D. F. Nelson and M. Lax, Phys. Rev. B **3**, 2795 (1971).

[2] A. Majchrowski, I. V. Kityk, T. Lukasiewicz, A. Mefleh, and S. Benet, Opt. Mater. (Amsterdam, Neth.) **15**, 51 (2000).

[3] A. Majchrowski, A. Mefleh, R. Lee, M. Makowska-Janusik, J. Kasperczyk, I. V. Kityk, J. Berdowski, and S. Benet, Mol. Cryst. Liq. Cryst. Sci. Technol., Sect. B: Nonlinear Opt. **24**, 335 (2000); I. V. Kityk, J. Zmija, A. Majchrowski, and J. Ebothe, J. Appl. Phys. **93**, 1160 (2002).

[4] V. I. Bielincher and B. I. Sturman, Usp. Fiz. Nauk **130**, 415 (1980); E. L. Ivczenko and G. E. Pikus, *Photogalvanic Effects in Semiconductors* (Nauka, Moscow, 1980), pp. 275–293.

[5] Santo Di Bella, Chem. Soc. Rev. **30**, 355 (2001); N. J. Long and C. K. Williams, Angew. Chem., Int. Ed. **42**, 2586 (2003); A. M. McDonagh, M. G. Humphrey, M. Samoc, B. Luther-Davies, S. Houbrechts, T. Wada, H. Sasabe, and A. Persoons, J. Am. Chem. Soc. **121**, 1405 (1999); S. Houbrechts, T. Wada, H. Sasabe, J. P. L. Morrall, I. R. Whittall, A. M. McDonagh, M. G. Humphrey, and A. Persoons, Mol. Cryst. Liq. Cryst. Sci. Technol., Sect. B: Nonlinear Opt. **22**, 165 (1999); A. M. McDonagh, M. G. Hum-phrey, M. Samoc, and B. Luther-Davies, Organometallics **18**, 5195 (1999).

[6] R. Blinc and B. Zeks, Adv. Phys. **21**, 693 (1972).

[7] A. Bussmann-Holder and H. Buttner, Nature (London) **360**, 541 (1992); N. Dalal, A. Klymachyov, and A. Bussmann-Holder, Phys. Rev. Lett. **81**, 5924 (1998).

[8] B. Sahraoui, I. V. Kityk, X. Nguyen Phu, P. Hudhomme, and A. Gorgues, Phys. Rev. B **59**, 9229 (1999); I. V. Kityk and B. Sahraoui, *ibid.* **60**, 942 (1999); H. Kaddouri, S. Benet, S. Char-rar, S. Tedenac, M. Makowska-Janusik, and I. V. Kityk, *ibid.* **62**, 17 108 (2000).

[9] D. Touchard, P. Haquette, A. Daridor, A. Romero, and P. H. Dix-neuf, Organometallics **17**, 3844 (1998); D. Touchard and P. H. Dixneuf, Coord. Chem. Rev. **178-180**, 409 (1998).

[10] K. Sonogashira, T. Yatake, Y. Tohda, S. Takahashi, and N. Hagi-hara, J. Chem. Soc., Chem. Commun. **135**, 291 (1977); K. So-nogashira, Y. Fujikura, T. Yatake, S. Takahashi, and N. Hagi-hara, J. Organomet. Chem. **145**, 101 (1978).

[11] T. J. J. Müller, Tetrahedron Lett. **38**, 1025 (1997); J. Organomet. Chem. **578**, 95 (1999).

[12] I. V. Kityk, B. Marciniak, and A. Mefleh, J. Phys. D **34**, 1 (2001).